Nanorods of Various Oxides and Hierarchically Structured Mesoporous Silica by Sol-Gel Electrophoresis

STEVEN J. LIMMER
Department of Materials Science and Engineering, University of Washington, Seattle, WA 98195, USA

TIMOTHY L. HUBLER
Pacific Northwest National Laboratory, Richland, WA 99352, USA

GUOZHONG CAO
Department of Materials Science and Engineering, University of Washington, Seattle, WA 98195, USA
gzcao@u.washington.edu

Abstract. In this paper, we report the template-based growth of nanorods of oxides and hierarchically structured mesoporous silica, formed by means of a combination of sol-gel processing and electrophoretic deposition. Both single metal oxides (TiO_2) and complex oxides ($Pb(Zr_{0.52}Ti_{0.48})O_3$) have been grown by this method. This method has also been applied to the growth of nanorods of mesoporous silica having an ordered pore structure, where the pores are aligned parallel to the long axis of the nanorod. Uniformly sized nanorods of about 125–200 nm in diameter and 10 μm in length were grown over large areas with near unidirectional alignment. Appropriate sol preparation yielded the desired stoichiometric chemical composition and crystal structure of the oxide nanorods, with a heat treatment (500–700°C for 15–30 min) for crystallization, densification and any necessary pyrolysis.

Keywords: sol-gel, electrophoresis, nanorods, complex oxides, mesoporous silica

Introduction

The synthesis of structures on the nanometer scale has been an area of increasing research activity in recent years. This includes the synthesis of materials with one (i.e., self-assembled monolayers), two (nanorods) or three (quantum dots) dimensions on the nanoscale. Many options are available for the synthesis of two-dimensional nanostructures. Demonstrated methods include a solution-phase method for the formation of Se nanowires [1] and formation of ribbon-like nanostructures of various oxides by thermal evaporation of oxide powders [2]. However, of the many methods available, few are suitable for the growth of nanostructured oxide materials, particularly of complex oxides. Examples include the formation of oxide nanorods by directly oxidizing metal nanorods [3] and direct template filling with oxide colloids [4]. We have recently demonstrated [5, 6] a method for combining sol gel processing with electrophoresis to grow nanorods of both single metal and complex oxides. This paper presents a further discussion of the technique, as well as the growth of ordered mesoporous silica.

Experimental

The chemicals used in making the sols were: titanium (IV) isopropoxide (97%), zirconium n-propoxide (70% in propanol), tetraethyl orthosilicate (98%), lead (II) acetate (99%), and *n*-hexadecyltrimethylammonium chloride (CTAC, 95%). Hydrochloric acid, glacial acetic acid, lactic acid, ethylene glycol, glycerol and ethanol were also used to adjust the pH and viscosity of the sols. The template membranes used for the growth of the nanorods were track-etched hydrophilic

polycarbonate, with a pore diameter 200 nm, and a thickness of 10 μm.

The formation of TiO_2 and $Pb(Zr_{0.52}Ti_{0.48})O_3$ (PZT) sols has been discussed previously [5, 6]. To prepare the mesoporous SiO_2 sol, CTAC was dissolved in a mixture of ethanol and DI water. TEOS and hydrochloric acid were added to the solution, which was stirred for 2 hrs at 25°C. The molar ratios used were approximately 1 TEOS: 1.5 EtOH: 1.8 H_2O: 0.07 HCl: 0.01 CTAC. The silica sol thus formed was rather stable, and took several weeks to gel at room temperature. The nanorod samples were prepared as previously described [6]. Scanning electron microscopy (SEM) and transmission electron microscopy (TEM) were used to study the morphology of the nanorods. X-ray diffraction (XRD) was used to determine the phases and crystal structures present, and to determine the pore sizes in the mesoporous silica sample.

Results

Figure 1 shows SEM and TEM images of TiO_2 nanorods that were grown by sol-gel electrophoresis. These samples were grown in a track-etched polycarbonate membrane with 200 nm diameter pores, and were fired at 500–700°C for 15 min. These nanorods have a uniform diameter throughout their entire length, with a surface that is smooth over much or all of the length. The diameter of the TiO_2 nanorods is ∼150 nm, which is approximately 25% smaller than the membrane pore diameter. This size difference is likely due to the shrinkage caused by densification during the heat treatment. Figure 1(b) also shows some broken rods, which appear solid and dense, as does the nanorod in the TEM image 1(c). This implies that the growth of the nanorods likely begins at the bottom of the pores, and proceeds from one side of the membrane to the other.
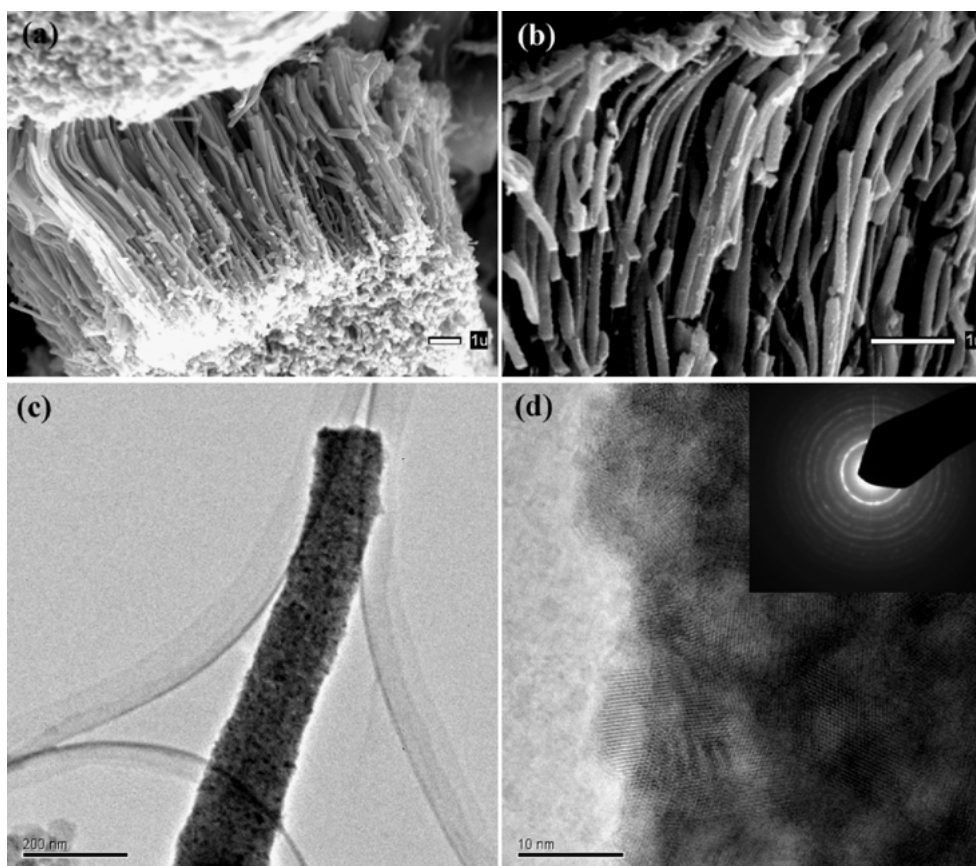
Figure 1.   SEM and TEM images of TiO_2 nanorods grown by sol-gel electrophoresis, showing a uniform diameter and smooth surface. The diameter of the TiO_2 nanorods is ∼150 nm, which is approximately 25% smaller than the membrane pore diameter. A high resolution TEM image and electron diffraction pattern are seen in part (d). They show that the nanorods are polycrystalline, with grains that are ∼5 nm in size.
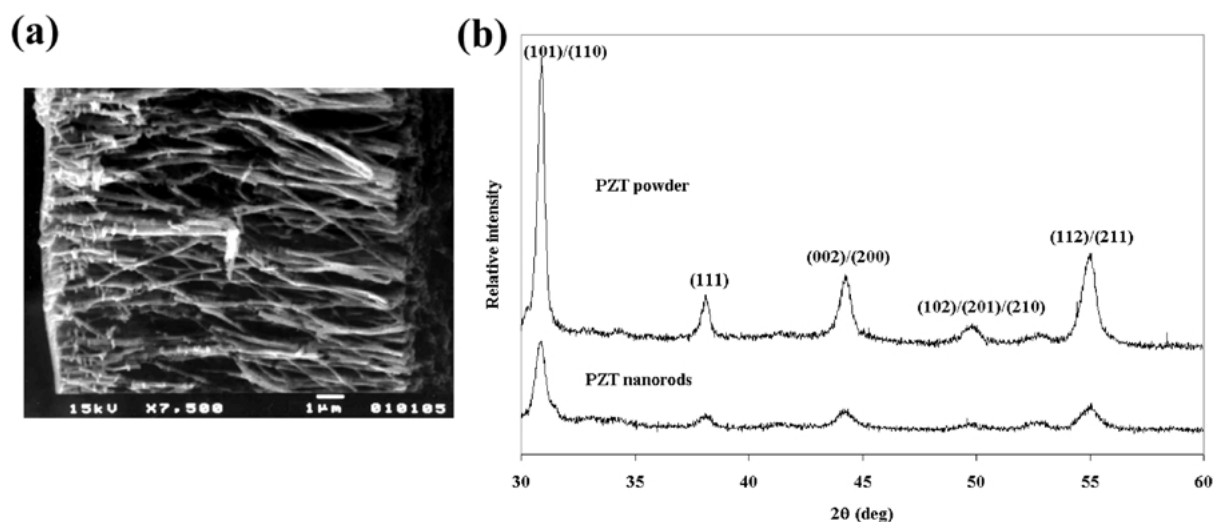
Figure 2. (a) shows an SEM micrograph of PZT nanorods. The PZT nanorods also have diameters of ~150 nm, and have a relatively smooth surface. (b) shows XRD spectra of the PZT nanorods and PZT powder prepared from the same sol; both the PZT nanorods and powder contain only the perovskite PZT phase.

A high resolution TEM image and electron diffraction pattern are shown in Fig. 1(d). They show that the nanorods are polycrystalline, with grains that are ~5 nm in size.

Figure 2 shows nanorods of PZT grown by sol gel electrophoresis. The PZT nanorods also have diameters of ~150 nm, which corresponds to shrinkage of about 25%. These nanorods also exhibit a uniform diameter throughout their entire length and have a rela-

tively smooth surface. Figure 2(b) shows XRD spectra of the PZT nanorods and PZT powder prepared from the same sol; both the PZT nanorods and powder contain only the perovskite PZT phase. Comparison of the two spectra shows that there are identical peaks in both samples, that the peak positions are the same, and that the intensity ratios among various peaks are identical. This demonstrates that electrophoretic deposition does not negatively affect the stoichiometry of the sol, and
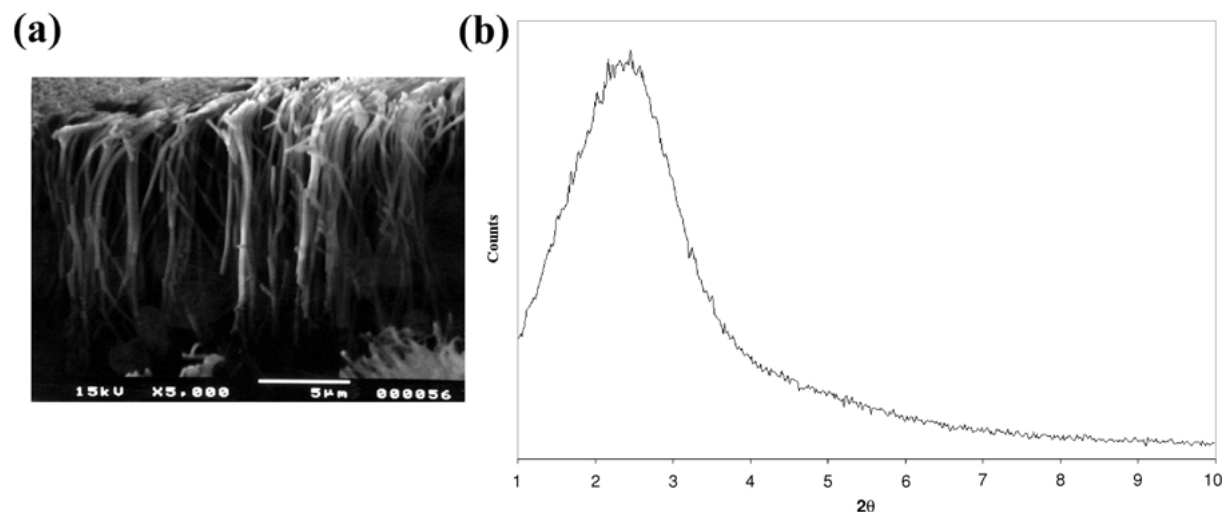
Figure 3. (a) shows an SEM micrograph of mesoporous silica nanorods. They are uniform in length and diameter. (b) is an XRD spectrum from a gelled and calcined sample of the sol used to make mesoporous SiO_2 nanorods. The spectrum shows a broad peak at 2.45° 2θ, which corresponds to a d_{100} spacing of about 3.7 nm.

thus can be used to form complex oxide rods of the desired phase and composition.

Figure 3 shows nanorods formed of mesoporous silica. They are uniform in length and diameter. Figure 3(b) is an XRD spectrum from a gelled and calcined sample of the sol used to make mesoporous SiO$_2$ nanorods. The spectrum shows a broad peak at 2.45° 2θ, which corresponds to a d_{100} spacing of about 3.7 nm. This agrees well with values reported in the literature for calcined samples of mesoporous silicas formed with CTAC as a surfactant [7]. The TEM image (not shown) shows that there are regions where the pores have a strong hexagonal ordering, as well as regions where they are more disordered. This disorder also shows up in the broad peaks of the XRD spectrum.

Discussion

A properly prepared sol contains solid nanoclusters of the desired stoichiometric chemical composition. If the sol is electrostatically stabilized, then the charged nanoclusters will have an oriented diffusion, parallel to the field direction, when an electric field is applied to the sol. This has been widely demonstrated as a method for growing thick films [8]. This electrophoretic motion is at the heart of the deposition technique we have used to grow nanorods. Figure 4 is a schematic drawing of the electrophoretic deposition process. It illustrates the steps we believe occur in the growth process. The nanoclusters will migrate and deposit at the bottom of the pore under an applied electric field. Simultaneously, the counter ions move in the opposite direction. As time increases, the densely packed sol particles fill more of the pore, until the pore is completely filled.

For the TiO$_2$ sol, the pH is ∼2, well below the isoelectric point (6.2) [9], and thus the particles would be positively charged, and the zeta potential would also be positive in a dilute sol. For PZT, since the pH of the sol (∼4) is below the reported isoelectric point (∼7.6) [10], the zeta potential is positive. In the SiO$_2$ sol, the pH is about 3, which is just above the isoelectric point (∼2), yielding negatively charged particles and a negative zeta potential.

If we assume that the nanoclusters are uniformly sized spheres, then the highest possible packing density is 74% [11]. This would also be the highest achievable density of the nanorods before densification. If there is a range of sizes in the nanoclusters, even denser packing could be possible. Upon heating the nanorods to an elevated temperature, densification will occur along
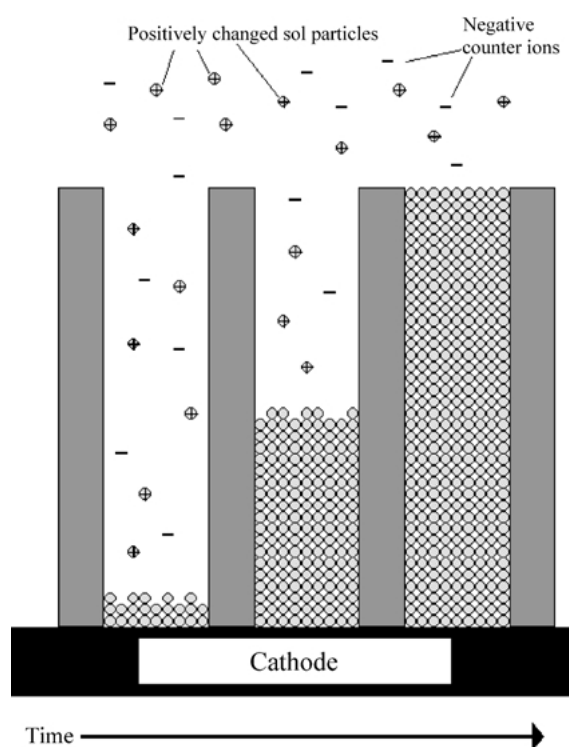
Figure 4. A schematic illustration of the growth process. First, on the left, charged sol particles are moving electrophoreticaly towards the electrode, depositing at the bottom of the pore. At the same time, counter ions are moving in the opposite direction. The center of the diagram shows a later time, as the densely packed sol particles fill up more of the pore. Lastly, the right side of the diagram shows a completely filled pore.

with shrinkage. This explains why the observed diameter of the nanorods is smaller than that of the membrane pores. Although we do not know how closely the nanoclusters packed during the electrophoretic deposition, a lateral shrinkage of approximately 25–30% was observed when the nanorods were fired.

It is known that the critical micelle concentration (CMC) of CTAC in a mixture of water and ethanol can be quite higher than it is in water alone [12]. Given the large amount of ethanol used in forming the silica-surfactant sol in this study, it is likely that the concentration is below CMC, and thus there would be no spontaneous formation of micelles in the bulk solution. However, self-assembly at the sol-substrate or sol-air interface commonly occurs [13]. The reported formation of mesoporous silica in microscopic channels and pores indicates that curvature promotes the cooperative self-assembly of micelles. In the current study, we have used a similar idea to that of Lu et al.

[14]; however, where that group used solvent evaporation to drive the concentration about CMC, we have used electrophoresis. Since both the (ionic) surfactant and the hydrolyzed and/or partially condensed silica precursor are charged in an electrolyte solution, they will move under an applied electric field, as has been demonstrated by Trau et al. [15]. The cationic surfactant species and the anionic silicate species likely join through electrostatic interactions in the sol. Since there is a far greater amount of silicate than surfactant, the net charge of the clusters will likely be negative. These charged coupled species assemble into micelle structures, specifically, hexagonal arrays of cylindrical micelles, promoted by both the curvature of the template pores and the electrophoretic enrichment of the solution inside the template pores.

Conclusions

In summary, we have demonstrated the applicability of sol-gel electrophoresis to the creation of various simple and complex oxide nanorods with a diameter ∼125–200 nm and a length of about 10 μm. This technique can also be used to form nanorods of hierarchically structured mesoporous silica.

Acknowledgments

References

1. B. Gates, Y. Yin, and Y. Xia, J. Am. Chem. Soc. **122**, 12582 (2000).
2. Z.W. Pan, Z.R. Dai, and Z.L. Wang, Science **291**, 1947 (2001).
3. Y. Li, G.S. Cheng, and L.D. Zhang, J. Mater. Res. **15**, 2305 (2000).
4. J.C. Hulteen and C.R. Martin, J. Mater. Chem. **7**, 1075 (1997).
5. S.J. Limmer, S. Seraji, M.J. Forbess, Y. Wu, T.P. Chou, C. Nguyen, and G.Z. Cao, Adv. Mater. **13**, 1269 (2001).
6. S.J. Limmer, S. Seraji, Y. Wu, T.P. Chou, C. Nguyen, and G.Z. Cao, Adv. Func. Mater. **12**, 59 (2002).
7. J.S. Beck, J.C. Vartuli, W.J. Roth, M.E. Leonowicz, C.T. Kresge, K.D. Schmitt, C.T.-W. Chu, D.H. Olson, E.W. Sheppard, S.B. McCullen, J.B. Higgins, and J.L Schlenker, J. Am. Chem. Soc. **114**, 10834 (1992).
8. K. Hasegawa, S. Kunugi, M. Tatsumisago, and T. Minami, J. Sol-Gel Sci. Tech. **15**, 243 (1999).
9. H. Hirashima, Y. Obu, T. Nagai, and H. Imai, Mat. Res. Soc. Symp. Proc. **346**, 95 (1995).
10. K. Baba, O. Nishizato, A. Takamura, and M. Katsube, J. Ceram. Soc. Jpn. **101**, 1370 (1993).
11. J.S. Reed, *Principles of Ceramic Processing* (Wiley, New York, 1995).
12. A. Cipiciani, G. Onori, and G. Savelli, Chem. Phys. Lett. **143**, 505 (1998).
13. H. Yang, N. Coombs, I. Sokolov, and G.A. Ozin, Nature **381**, 589 (1996).
14. Y. Lu, R. Ganguli, C.A. Drewien, M.T. Anderson, C.J. Brinker, W. Gong, Y. Guo, H. Soyez, B. Dunn, M.H. Huang, and J.I. Zink, Nature **389**, 364 (1997).
15. M. Trau, N. Yao, E. Kim, Y. Xia, G.M. Whitesides, and I.A. Aksay, Nature **390**, 674 (1997).